

Article

Superhydrophobic Surfaces Boost Fibril Self-Assembly of Amyloid β PeptidesAngelo Accardo, Victoria Shalabaeva, Emanuela Di Cola, Manfred
Burghammer, Roman Krahnke, Christian Riekkel, and Silvia DanteACS Appl. Mater. Interfaces, **Just Accepted Manuscript** • DOI: 10.1021/acsami.5b06219 • Publication Date (Web): 26 Aug 2015Downloaded from <http://pubs.acs.org> on September 3, 2015**Just Accepted**

“Just Accepted” manuscripts have been peer-reviewed and accepted for publication. They are posted online prior to technical editing, formatting for publication and author proofing. The American Chemical Society provides “Just Accepted” as a free service to the research community to expedite the dissemination of scientific material as soon as possible after acceptance. “Just Accepted” manuscripts appear in full in PDF format accompanied by an HTML abstract. “Just Accepted” manuscripts have been fully peer reviewed, but should not be considered the official version of record. They are accessible to all readers and citable by the Digital Object Identifier (DOI®). “Just Accepted” is an optional service offered to authors. Therefore, the “Just Accepted” Web site may not include all articles that will be published in the journal. After a manuscript is technically edited and formatted, it will be removed from the “Just Accepted” Web site and published as an ASAP article. Note that technical editing may introduce minor changes to the manuscript text and/or graphics which could affect content, and all legal disclaimers and ethical guidelines that apply to the journal pertain. ACS cannot be held responsible for errors or consequences arising from the use of information contained in these “Just Accepted” manuscripts.

1
2
3
4
5
6
7
8
9
10
11
12
13
14
15
16
17
18
19
20
21
22
23
24
25
26
27
28
29
30
31
32
33
34
35
36
37
38
39
40
41
42
43
44
45
46
47
48
49
50
51
52
53
54
55
56
57
58
59
60

Superhydrophobic Surfaces Boost Fibril Self-Assembly of Amyloid β Peptides

Angelo Accardo^{a,}, Victoria Shalabaeva^a, Emanuela Di Cola^{b,1}, Manfred Burghammer^b, Roman Krahne^a, Christian Riek^b and Silvia Dante^a*

^a *Istituto Italiano di Tecnologia, Via Morego 30, Genova 16163, Italy*

^b *The European Synchrotron, CS40220, 38043 Grenoble Cedex 9, France*

**Corresponding author's e-mail address: angelo.accardo@iit.it*

¹*Current address: Laboratoire Interdisciplinaire de Physique (LIPhy UMR5588 CNRS/UJF), 140 rue de la Physique, BP87 38402 Saint Martin d'Hères Cedex.*

KEYWORDS: Superhydrophobic, Convective flows, β -amyloid, Fibril self-assembly, X-ray diffraction, Synchrotron radiation.

1
2
3 ABSTRACT
4

5 Amyloid β ($A\beta$) peptides are the main constituents of Alzheimer's amyloid plaques in the brain.
6
7 Here we report how the unique microfluidic flows exerted by droplets sitting on
8
9 superhydrophobic surfaces can influence the aggregation mechanisms of several $A\beta$ fragments
10
11 by boosting their fibril self-assembly. $A\beta(25-35)$, $A\beta(1-40)$ and $A\beta(12-28)$ were dried both on
12
13 flat hydrophilic surfaces (contact angle, $CA=37.3^\circ$) and on nanostructured superhydrophobic
14
15 ones ($CA=175.8^\circ$). By embedding nanoroughened surfaces on top of highly X-ray transparent
16
17 Si_3N_4 membranes, it was possible to probe the solid residues by raster-scan synchrotron radiation
18
19 X-ray micro-diffraction (μ XRD). As compared to residues obtained on flat Si_3N_4 membranes, a
20
21 general enhancement of fibrillar material was detected for all $A\beta$ fragments dried on
22
23 superhydrophobic surfaces, with a particular emphasis on the shorter ones. Indeed, both $A\beta(25-$
24
25 $35)$ and $A\beta(12-28)$ showed a marked crystalline cross- β phase with varying fiber textures. The
26
27 homogeneous evaporation rate provided by these nanostructured supports, and the possibility to
28
29 use transparent membranes, can open a wide range of *in-situ* X-ray and spectroscopic
30
31 characterizations of amyloid peptides involved in neurodegenerative diseases and for the
32
33 fabrication of amyloid-based nanodevices.
34
35
36
37
38
39
40
41
42
43
44
45
46
47
48
49
50
51
52
53
54
55
56
57
58
59
60

Introduction

Amyloids are insoluble protein aggregates which are the main cause of more than twenty human diseases.^{1,2} Among these amyloid-dependent syndromes are neurodegenerative pathologies such as Alzheimer's,³ Parkinson's⁴ and Huntington's diseases⁵ but also non-neuropathic localized amyloidosis such as diabetes mellitus type II.^{6,7} Several approaches and innovative techniques have been used in the last decades to monitor the mechanisms which lead to the formation of the fibrils that are at the base of the above mentioned diseases.⁸⁻¹³ Considering how the number of patients affected by dementia will triple by 2050,¹⁴ going from the actual 45 million to more than 135 million, the role of Alzheimer's disease (AD) assumes huge social implications. AD is characterized by the formation of extracellular amyloidal plaques, rich in fibrils of A β (1-40) and A β (1-42), which may act also as reservoir for the most toxic A β membrane-soluble species, such as oligomers and protofibrils.^{15,16} A more detailed knowledge of the aggregation path differentiation for the various A β species and of the final structure adopted by their fibers can add new information about the role of the different A β s in the neurodegenerative mechanisms.

Our aim is showing that amyloid fibrillation mechanisms can be sensitively affected by the presence of superhydrophobic and superhydrophilic surfaces and materials.¹⁷⁻²⁰ Indeed, molecular self-assembly has been demonstrated for a wide range of materials and mechanisms of biological interest¹⁷ such as synthetic amyloid peptides,^{21,22} protein conformational changes,^{18,23} biomineralization processes,²⁴ nanocrystallization,²⁵ DNA pulling,²⁶ and healthy/tumoral cell exosomes discrimination.²⁷ For droplets on hydrophilic surfaces, the evaporation rate is highest at the triple contact-line resulting in an outward convective flow, while droplets on superhydrophobic surfaces (SHSs) have a more homogeneous evaporation rate across their surface resulting in the presence of a circulatory convective flow.¹⁷ The flows generated inside

1
2
3 evaporating drops on SHSs can then be used to induce ordering effects in the analyte as observed
4
5 for the formation of fibrillar lysozyme related to a local convective flow field developed during
6
7 pinning of the drying drop at the interface between the droplet and the substrate.²⁸ Further,
8
9 synthetic trimeric to hexameric peptides show residues with marked cross- β sheet configuration
10
11 after evaporation of quasi contact-free droplets on superhydrophobic surfaces.^{21,22} Under the
12
13 same conditions, lysozyme in presence of Ca^{2+} ions and a weakly acidic environment, self-
14
15 assembles also into a fibrillar amyloidic phase on a time scale much shorter than that reported in
16
17 literature.²³ On the other hand, several $\text{A}\beta$ fragments, which are directly involved in the
18
19 formation of AD plaques in the brain, show a direct correlation between secondary structure
20
21 conformational changes, presence of nanostructured surfaces and peptide concentration.^{18,19}
22
23 Besides amyloidal proteins involved in different pathologies, there is also a class of self-
24
25 assembling peptides which, thanks to their low immunogenic and inflammatory potential, are at
26
27 the center of a fascinating research branch which aims at different applications in the field of
28
29 nanobiotechnology.^{29,30} Among these “functional amyloids” are prion-related ones which are
30
31 essential for the storage of memory in the brain,³¹ amyloid fibers that serve as templates for the
32
33 biosynthesis of melanin^{32,33} and amyloid fibrils employed as biomaterial for promoting cell
34
35 adhesion, migration and differentiation.³⁴ Considering all these aspects, the existence of a
36
37 protocol able to control the formation of fibril-self assembly in such bio-compounds would be
38
39 crucial not just for better understanding the formation of amyloid material in neurodegenerative
40
41 and non-neurodegenerative diseases, but could also be exploited as a versatile fabrication
42
43 approach of novel biomaterials for biomedicine and tissue engineering purposes.
44
45
46
47
48
49
50
51

52
53 The ability to manipulate biological soft matter aggregation has been exploited in this work to
54
55 guide the process of fibril self-assembly in $\text{A}\beta$ proteins by the peculiar microfluidic flows
56
57
58
59
60

1
2
3 induced by biomimetic SHSs, which mimic lotus leaves superhydrophobic features. For this aim
4 we embedded poly(methyl methacrylate) (PMMA) nanostructuresd SH coatings on ultrathin
5
6 Si₃N₄ membranes in order to perform *in-situ* X-ray micro-diffraction (μ XRD) studies on the
7
8 dried residues. Following this approach we made a comparative evaluation of different amyloid
9
10 β -peptides, namely A β (25-35), A β (1-40) and A β (12-28), confined in droplet environments
11
12 both on flat hydrophilic Si₃N₄ membranes and on SH ones. While on hydrophilic supports it is
13
14 possible to observe characteristic ring-like moieties already studied elsewhere,^{18,19,35} the
15
16 homogeneous evaporation rate provided by superhydrophobic surfaces¹⁷ induce the formation of
17
18 freestanding samples. As compared to flat Si₃N₄ membranes, A β fragments in presence of
19
20 superhydrophobic supports result in a strong enhancement of the fibrillar component, often
21
22 accompanied by a quasi-crystalline structure. We show that raster-scan diffraction with a
23
24 micrometric synchrotron radiation X-ray beam is required for revealing local super-structures
25
26 with variable fiber textures. The control over the aggregation mechanisms of fibril self-assembly
27
28 in natural peptides, provided by the use of the protocol presented in this study, is a valuable tool
29
30 both to shed more light on the processes resulting in the formation of amyloid fibrils in
31
32 neurodegenerative diseases and as a fabrication route for the development of amyloidal films to
33
34 be used in the field of biomedicine. In this work we present a new class of superhydrophobic X-
35
36 ray transparent Si₃N₄ membranes allowing to investigate the effects of convective flows in μ L
37
38 droplets on the self-assembly mechanisms of amyloid- β peptides involved in Alzheimer's
39
40 disease by μ XRD.
41
42
43
44
45
46
47
48
49
50

51 **Experimental section**

52 **A β Peptides.** A β (1-40) (H-Asp-Ala-Glu-Phe-Arg-His-Asp-Ser-Gly-Tyr-Glu-Val-His-His-Gln-
53
54 Lys-Leu-Val-Phe-Phe-Ala-Glu-Asp-Val-Gly-Ser-Asn-Lys-Gly-Ala-Ile-Ile-Gly-Leu-Met-Val-
55
56
57
58
59
60

1
2
3 Gly-Gly-Val-Val-OH, molecular formula $C_{194}H_{295}N_{53}O_{58}S$), A β (12-28) (H-Val-His-His-Gln-
4
5 Lys-Leu-Val-Phe-Phe-Ala-Glu-Asp-Val-Gly-Ser-Asn-Lys-OH, molecular formula
6
7 $C_{89}H_{135}N_{25}O_{25}$) and A β (25-35) (H-Gly-Ser-Asn-Lys-Gly-Ala-Ile-Ile-Gly-Leu-Met-OH,
8
9 molecular formula $C_{45}H_{81}N_{13}O_{14}S$) fragments were products of Bachem. The peptides were first
10
11 dissolved in trifluoroacetic acid (TFA) at a concentration of 1 mg/mL to eliminate the presence
12
13 of seeds and to obtain a monomeric peptide dispersion. TFA was dried under nitrogen, and the
14
15 peptides were successively dissolved in Milli-Q water (1 mg/mL), shortly sonicated, and
16
17 centrifuged at 10000 RPM for 10 min.
18
19
20
21

22
23 **Superhydrophobic Si₃N₄ membranes fabrication.** Si₃N₄ – Si – Si₃N₄ <100> wafers (Si
24
25 thickness 525 μ m, Si₃N₄ thickness 500 nm) were purchased from University Wafer. We adopted
26
27 an optical lithography process in order to obtain a matrix of single square Si₃N₄ membranes of 5
28
29 mm x 5 mm size. After spin-coating the wafer with S1813 positive resist at 4000 RPM for 60 s,
30
31 the wafer went through a baking process (90°C for 3 minutes). UV exposure was performed with
32
33 a SUSS MicroTech mask-aligner in soft contact for 15 seconds and it was followed by a MF319
34
35 development for 1 minute. A reactive ion etch process (Sentech 500 system, CHF₃ 70 sccm, O₂ 5
36
37 sccm, RF 70 W, ICP 200 W, P = 1 Pa) allowed to etch the Si₃N₄ regions not covered by the
38
39 optical resist. The residual resist was then stripped by cold acetone (5 min) and the entire wafer
40
41 passed through a wet etch based on KOH (100 g of KOH in 150 ml of H₂O at 105°C) for 6-8
42
43 hours. After etching the Si, the wafer was rinsed in milliQ water and baked at 65°C to dry it
44
45 completely before performing the superhydrophobic coating. The wafer was spin-coated with
46
47 PMMA A11 (MicroChem) resist at 2000 RPM for 60s and baked (180°C for 30 min) obtaining
48
49 an homogenous layer of 1 μ m thickness. A further plasma reactive ion etching process was
50
51 employed to nanotexture the PMMA layer (ICP 50 W, RF 100 W, P = 6.5 Pa, O₂ 30 sccm, 5
52
53
54
55
56
57
58
59
60

1
2
3 min) and to deposit a thin layer of Teflon on top of it (RF 600 W, P = 3.6 Pa, C₄F₈ 85 sccm, 5 s).

4
5
6
7 **Contact Angle measurements.** The evaluation of aqueous droplets contact angle was estimated
8
9 using a Kruss DSA100 setup, yielding a value of $37.3^\circ \pm 0.5^\circ$ in presence of flat pristine Si₃N₄
10 supports and $175.8^\circ \pm 0.5^\circ$ in presence of superhydrophobic Si₃N₄ supports (Supporting
11 Information, Figure S1).
12
13
14

15
16
17 **Synchrotron Radiation Experiments.** μ XRD experiments were performed at the ID13
18 Microfocus beamline of the European Synchrotron Radiation (ESRF). A monochromatic beam
19 of $\lambda = 0.0968633$ nm was focused to a $2.5(v) \times 2.8(h)$ μm^2 with about 3×10^{11} photons/s flux at
20 the sample position using a transfocator³⁶ based on parabolic Be-refractive lenses. A Frelon CCD
21 detector with 2048 \times 2048 pixels of 50×50 μm^2 each (binned to 4 \times 4) was used for data collection
22 with an exposure of 0.5 s per pattern. The sample-to-detector distance was evaluated to be 142.1
23 mm by an Ag-behenate calibrant. Regions of interest of the sample were selected using an on-
24 axis optical Olympus microscope aligned with the focal spot of the microbeam. The expression
25 of the scattering vector Q in the illustrated azimuthal averages is equal to $Q = 4\pi \sin \theta / \lambda$, where
26 θ is the diffraction angle and λ is the X-ray wavelength. FIT2D and an ID13 beamline in-house
27 developed software have been used for data analysis.
28
29
30
31
32
33
34
35
36
37
38
39
40
41
42

43
44 **Scanning Electron Microscopy (SEM).** SEM images were recorded by a FEI HELIOS Nanolab
45 600 instrument with a 10 kV acceleration voltage on samples sputtered with a 10 nm layer of
46 gold.
47
48
49
50

51 52 **Results and discussion**

53
54 Figure 1A illustrates the typical experimental configuration of the μ XRD experiments. After
55 evaporation of 5 μL droplets of A β aqueous solutions (1 mg/mL) either on the superhydrophobic
56
57
58
59
60

1
2
3
4
5
6
7
8
9
10
11
12
13
14
15
16
17
18
19
20
21
22
23
24
25
26
27
28
29
30
31
32
33
34
35
36
37
38
39
40
41
42
43
44
45
46
47
48
49
50
51
52
53
54
55
56
57
58
59
60

Si_3N_4 membranes (Figure 1B,C) or on the flat pristine hydrophilic ones, the windows were mounted on a goniometer in front of a highly collimated X-ray beam to perform μXRD analysis (see Methods, Figure 1A and Figure S1) in transmission geometry exploiting the X-ray transparency of the membrane. In all the experiments that we performed we evidenced a sharp difference between the residues obtained on superhydrophobic and hydrophilic supports. On the latter ones we obtained ring-like residues very adherent to the surface (Figure 2A-4A) confirming how the evaporation flux configuration on a hydrophilic surface induces an outward convective flow, a pinning of the droplet and the formation of a coffee-ring residue.³⁵

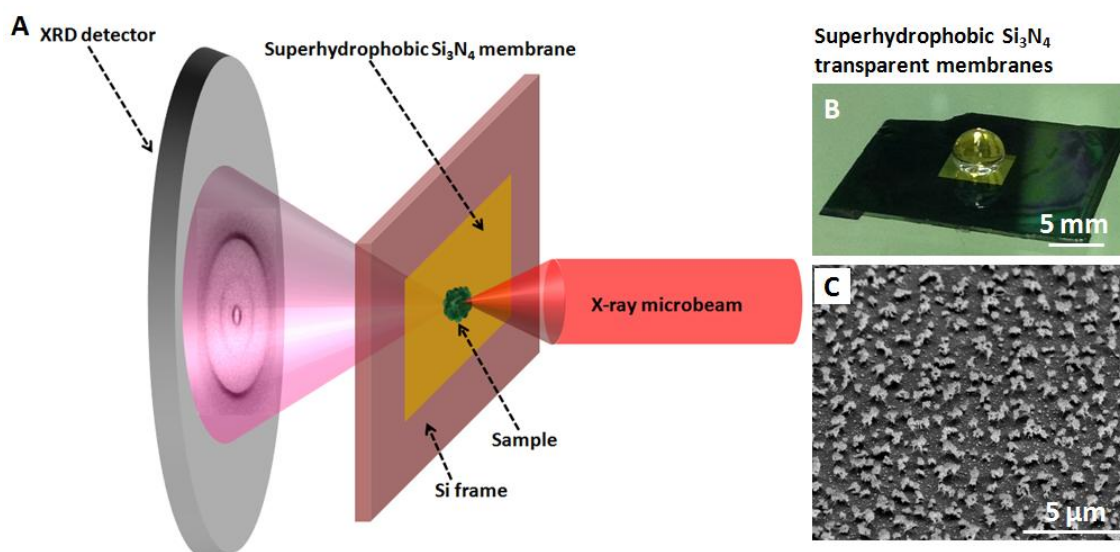


Figure 1 A: Sketch of the experimental setup in the ID13 microfocus beamline with the X-ray beam impinging the sample formed over the superhydrophobic membrane and resulting in a scattering pattern recorded by the XRD detector (the experimental environment of the beamline is shown in figure S1); B: Aqueous droplet sitting on a superhydrophobic Si_3N_4 membrane; C: SEM micrograph evidencing the rough morphology of the PMMA coating on the superhydrophobic Si_3N_4 membranes.

On the contrary, the presence of recirculating convective flows, of an extremely homogenous evaporation rate and of a low interaction between the droplet and the underneath superhydrorepellent surface¹⁷ induced the formation of free standing tridimensional residues (Figure 5A-7A).

μ XRD analysis of the A β peptides dried on flat Si₃N₄ membranes.

Figure 2A shows the optical image of a typical ring-like residue obtained from A β (25-35) peptide dried on a flat Si₃N₄ membrane. The inset shows the morphology of the external rim while Figure 2B illustrates a μ XRD mesh scan of such region where each single “pixel” is a XRD pattern covering a 2.5(v) \times 2.8(h) μ m² area according to the beam spot-size (see Methods).

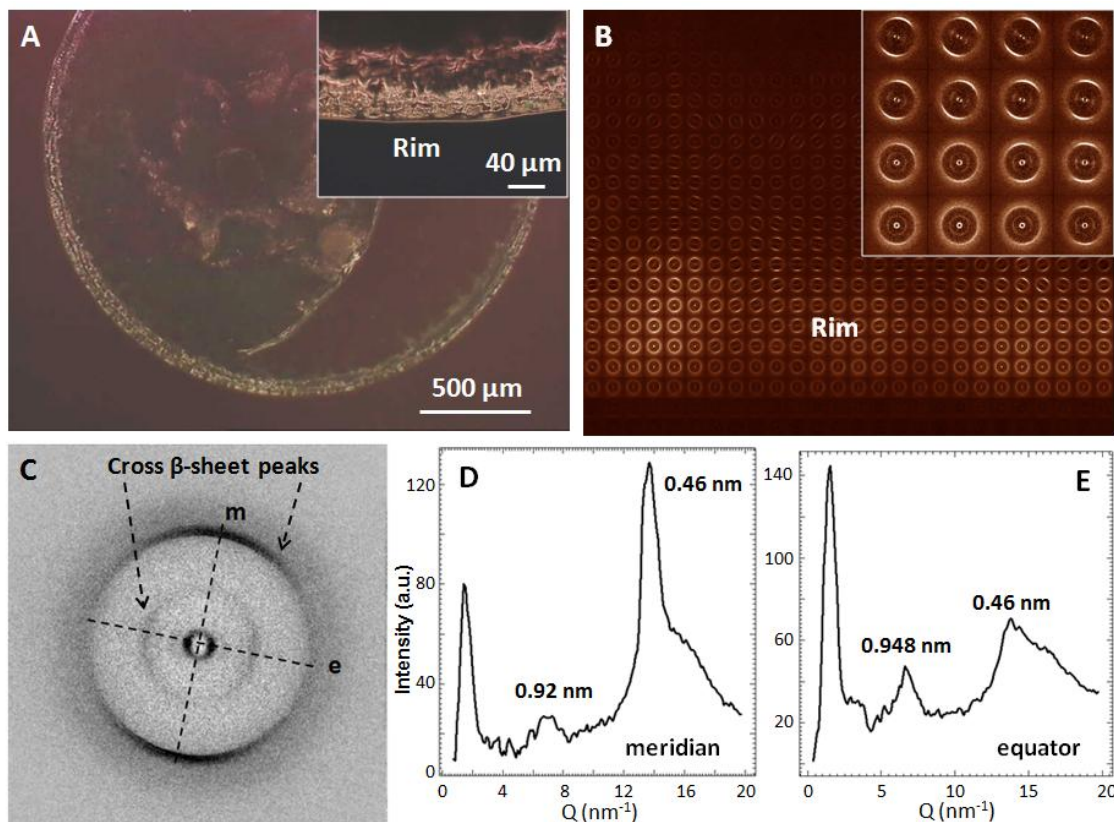


Figure 2 A: Optical image of A β (25-35) ring-like residue dried on a flat Si₃N₄ membrane (inset: close-up on the rim of the residue); B: μ XRD mesh scan of a portion of the rim in figure 2A (inset: close up on a few μ XRD patterns); C: Typical orthogonal μ XRD pattern from the rim of the residue highlighting the meridional and equatorial directions; D,E: Azimuthal averages of the μ XRD pattern of Figure 2C along the meridian (D) and equatorial (E) directions.

This peptide has been extensively studied in previous works^{18,19} on superhydrophilic surfaces where it showed a concentration-dependant α -helical to β -sheet transition. As shown by a typical XRD pattern of the rim (Figure 2C), in presence of a conventional hydrophilic surface, such as flat Si₃N₄, we have the presence of a distinct cross- β sheet structure exhibiting a meridional d =

1
2
3 0.46 nm spacing (azimuthal average in Figure 2D), related to the distance between hydrogen-
4 bonded strands, and an equatorial spacing of 0.948 nm (azimuthal average in Figure 2E),
5 characteristic of β -sheet stacking. This configuration is universally recognized as the gold
6 standard to unmistakably define amyloid fibrils.²
7
8
9
10
11

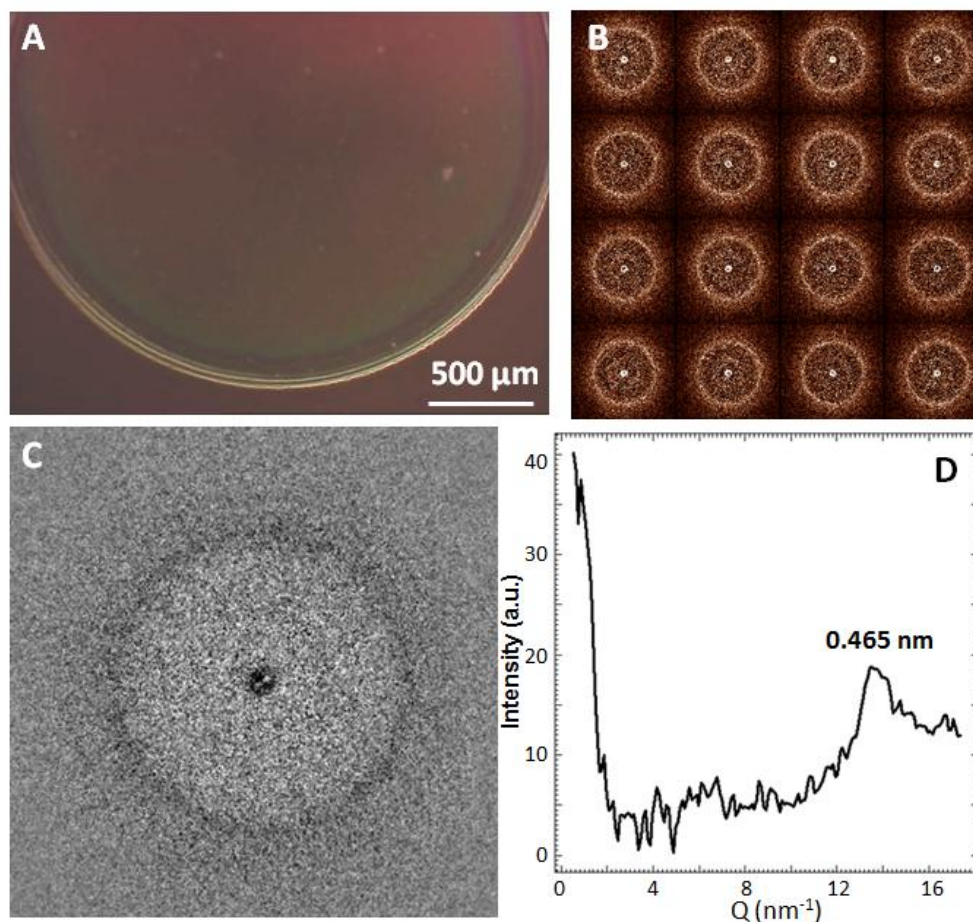


Figure 3 A: Optical image of $A\beta(1-40)$ ring-like residue dried on a flat Si_3N_4 membrane; B: μ XRD mesh scan of a portion of the rim in figure 3A; C: Typical μ XRD pattern from the rim of the residue; D: Azimuthal average of the μ XRD pattern of Figure 3C.

As demonstrated in previous works, the kinetics and amyloid morphology of $A\beta$ peptides can be significantly different.³⁷ As further confirmation of these differences, $A\beta(1-40)$ peptide showed a very different structure on flat supports if compared with the $A\beta(25-35)$ one. Although the morphology of the residue looked very similar to the one of $A\beta(25-35)$ (Figure 3A), the typical XRD patterns (Figure 3B,C) revealed only an unordered β -type phase with a weak contribution

at $d \approx 0.465$ nm (Figure 3D), related to hydrogen-bonded strands. A similar configuration was found for the fragment A β (12-28) (Figure 4A-E) even though in this case we detected a quite sharp fibril orientation (Figure 4C).

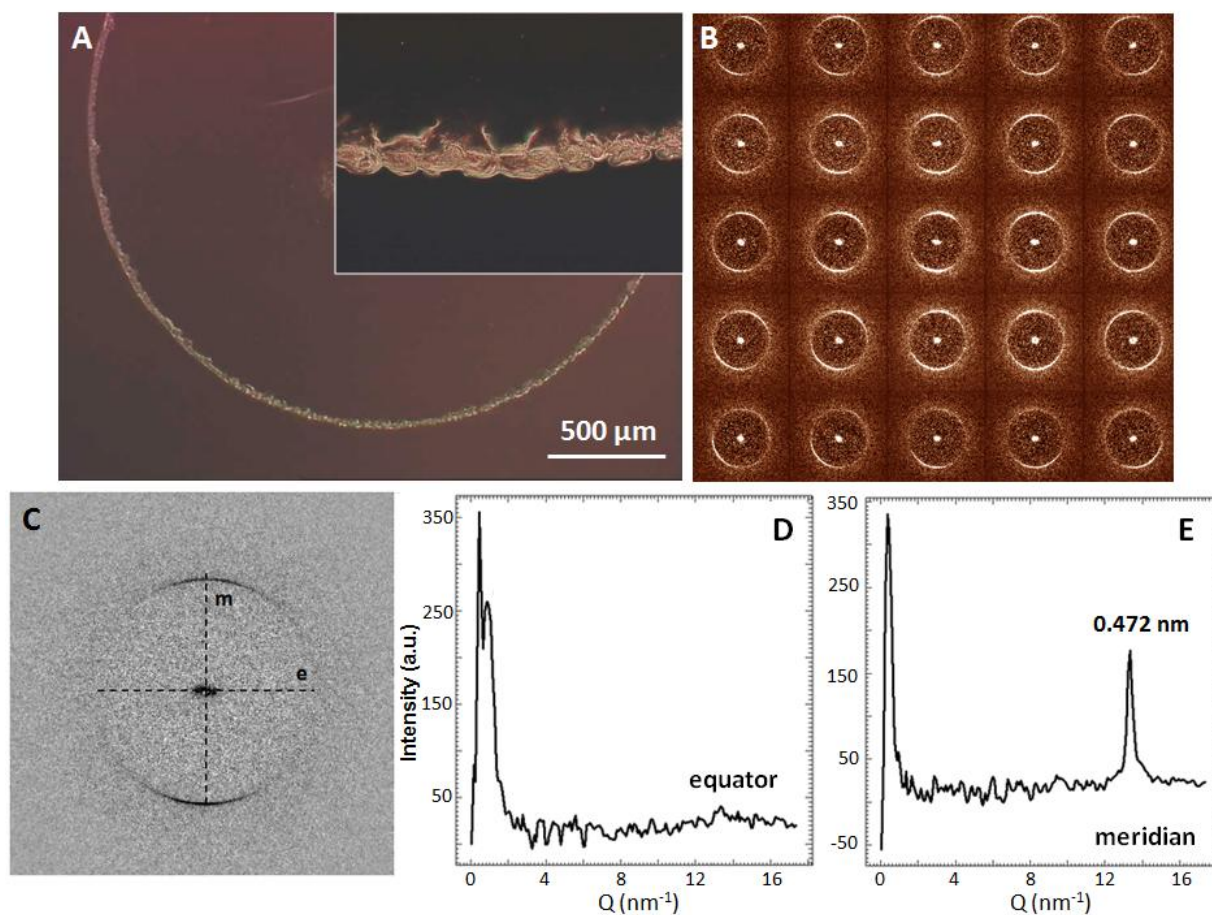
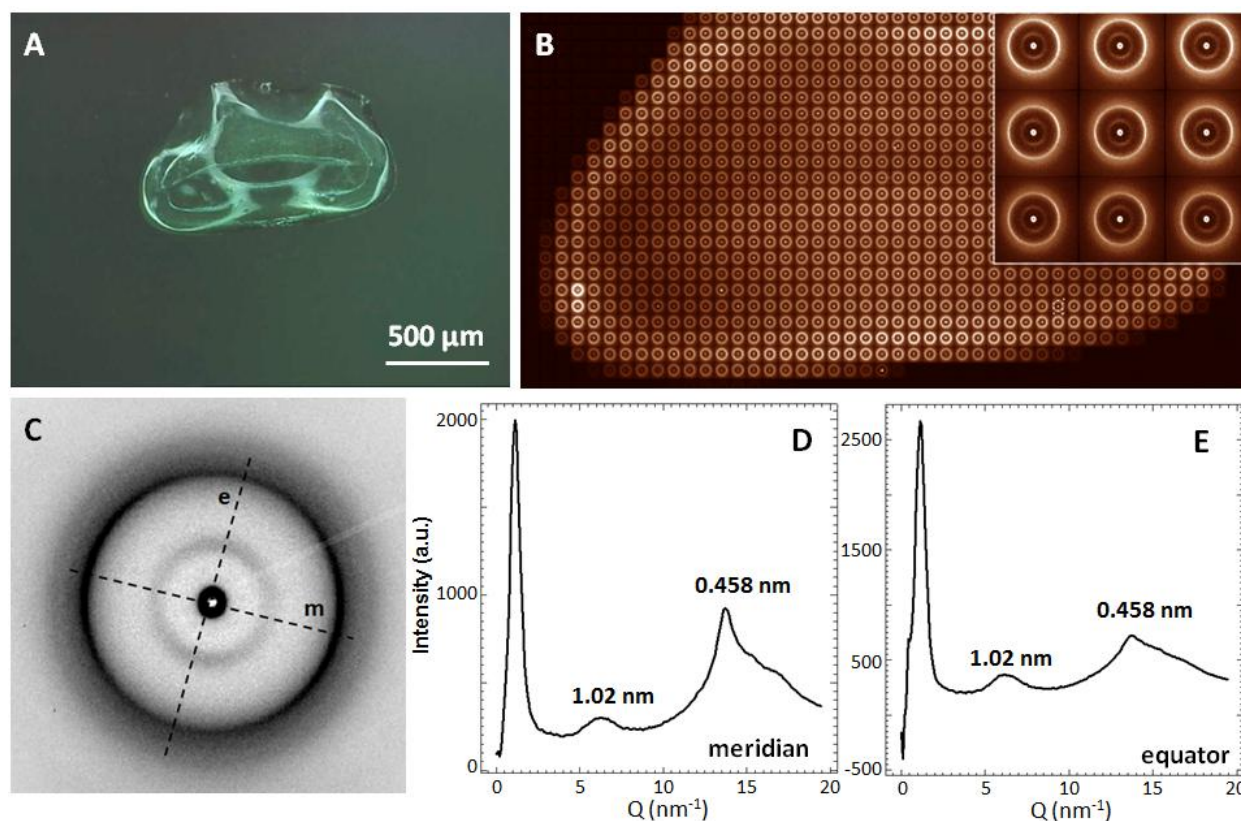


Figure 4 A: Optical image of A β (12-28) ring-like residue dried on a flat Si₃N₄ membrane (inset: close-up on the rim of the residue); B: μ XRD mesh scan of a portion of the rim in figure 4A; C: Typical μ XRD pattern from the rim of the residue highlighting the meridional and equatorial directions; D,E: Azimuthal averages of the μ XRD pattern of Figure 4C along the equatorial (D) and meridian (E) directions.

As shown by the XRD mesh scan and the single XRD pattern, respectively, in Figures 4B,C, the rim showed several areas with marked β -sheet conformation with a strongly oriented meridional reflection at $d \approx 0.472$ nm (Figure 4E). As happened for the A β (1-40) peptide, also in this case there was no appearance of the ≈ 1 nm reflection characteristic of β -sheet stacking, suggesting a possible stacking disorder.

1
2
3
4 It is worth noting that the aggregation kinetics of the investigated fragments, *i.e.*, their
5 conversion from non-amyloidogenic to amyloidogenic forms, differs significantly. In particular,
6 for A β (1-40), which in aqueous solution, at physiological conditions, has a partially unfolded
7 structure,³⁸ fibrillogenesis is rather low and may occur in several hours, depending on its
8 concentration,^{37,39} on the contrary the undecapeptide A β (25-35), which is the shorter A β
9 fragment retaining the toxic characteristic of the full length A β peptide, shows a very rapid self-
10 assembly behavior.⁴⁰ These differences reflect distinct aggregation paths and possibly the
11 presence of different intermediates, which may therefore aggregate in diverse molecular
12 architectures, as indicated by our findings.



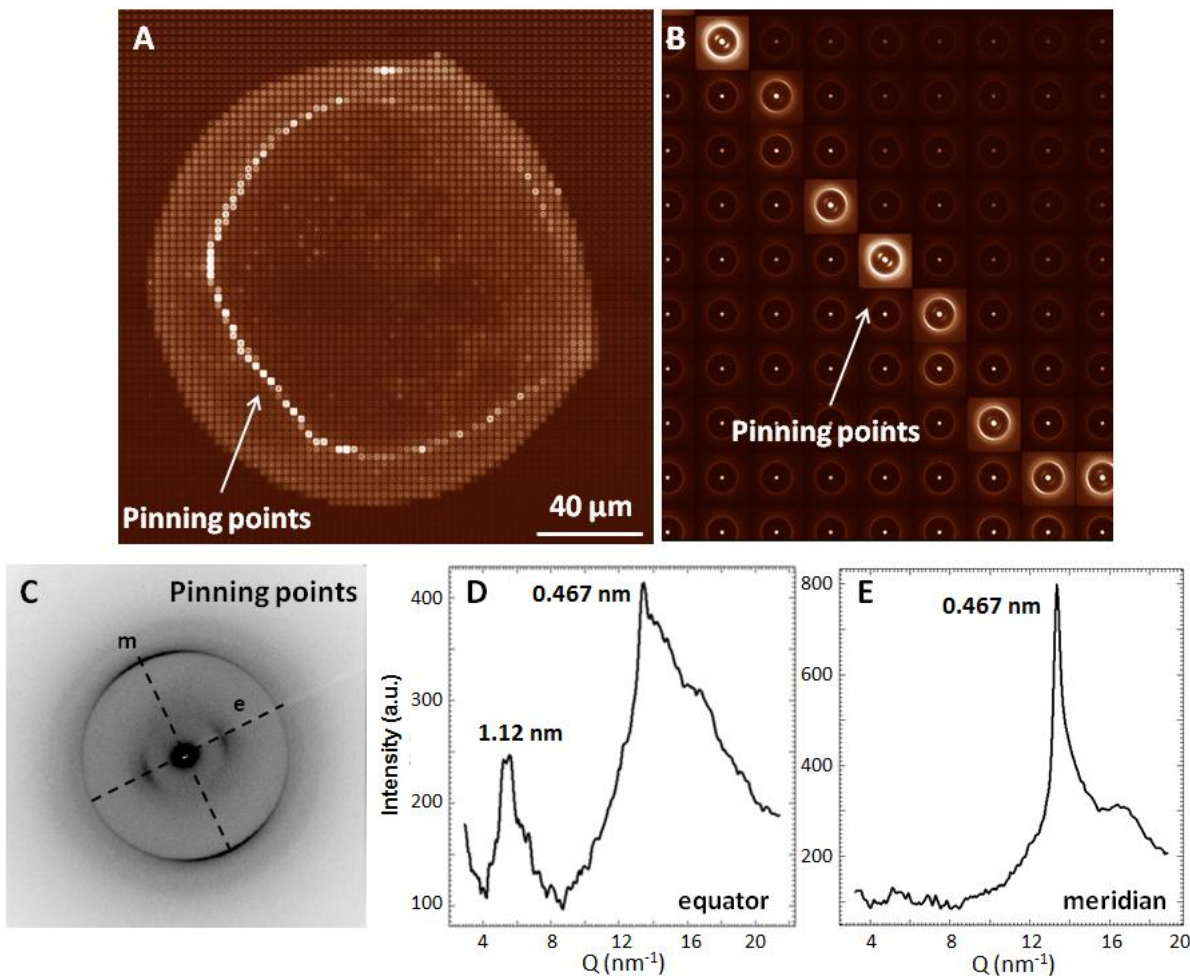
37
38
39
40
41
42
43
44
45
46
47
48
49
50
51
52
53
54
55
56
57
58
59
60
Figure 5 A: Optical image of A β (1-40) free-standing residue dried on a superhydrophobic Si₃N₄ membrane; B: μ XRD mesh scan of the residue in figure 5A (inset: close up on a few μ XRD patterns); C: Typical μ XRD pattern of the residue highlighting the meridian and equatorial directions; D,E: Azimuthal averages of the μ XRD pattern of Figure 5C along the meridian (D) and equatorial (E) directions.

μ XRD analysis of the A β peptides dried on superhydrophobic Si₃N₄ membranes.

The conformation of the analyzed β -amyloid peptides changes abruptly in presence of the superhydrophobic X-ray transparent supports. The optical image in figure 5A shows a typical free-standing residue of a A β (1-40) solution droplet dried on the superhydrophobic surface. The μ XRD raster-scan (Figure 5B) reveals a β -type fiber texture contrasting the weak unoriented powder-like β -type material obtained in the hydrophilic case (Figure 3). In particular the azimuthal averages along the equatorial and meridional directions (Figure 5D,E) of a typical XRD pattern (Figure 5C) extracted from the mesh scan, highlights the presence of an orthogonal cross β -sheet configuration with the characteristic reflections at 1.02 nm and 0.458 nm. This result shows how, on very short time scales (each evaporation of a 5 μ L droplet takes around 1 h), it is possible to boost the self assembly of amyloid fibrils of an A β peptide which, dried on conventional flat hydrophilic surfaces, does not show any ordered fibril structure. This can be attributed to the peculiar microfluidic flows and the homogeneous evaporation rate provided by droplets sitting on superhydrophobic supports that give enough time to the analyte to arrange in a gradual and more ordered way if compared with the hydrophilic substrate. In this latter case indeed the evaporation rate is very strong at the edge of the droplet and very low at the center, inducing a faster, but highly heterogeneous, evaporation rate which pushes the analyte to aggregate just at the rim of the solid residue.^{18,19,35}

This “boosting” effect becomes even more evident with the shorter peptides under investigation. Figure 6A shows a XRD mesh scan of the A β (12-28) peptide for which we obtained a free-standing residue characterized again by highly oriented amyloid fibril patterns as better shown in Figure 6B,C. Albeit in presence of a hydrophilic support we already observed the presence of oriented patterns (Figure 4), in that case we could detect only the typical meridional

1
2
3 reflection at $d \approx 0.472$ nm characteristic of hydrogen-bonded strands. On the contrary, in the
4
5 superhydrophobic case it is possible to appreciate the presence of a very well defined region of
6
7 the residue where the typical XRD patterns (Figure 6C) show a marked cross β -sheet
8
9 configuration including, besides the $d \approx 0.467$ nm reflection, also the orthogonal $d \approx 1.12$ nm one
10
11 related to β -sheet stacking (Figure 6D,E).



47 Figure 6 A: μ XRD mesh scan of the $A\beta(12-28)$ residue dried on a superhydrophobic Si_3N_4 membrane; B: close up
48 on the μ XRD patterns located in proximity of the droplet pinning points; C: Typical μ XRD pattern of the residue
49 highlighting the meridional and equatorial directions; D,E: Azimuthal averages of the μ XRD pattern of Figure 6C
50 along the equatorial (D) and meridian (E) directions.

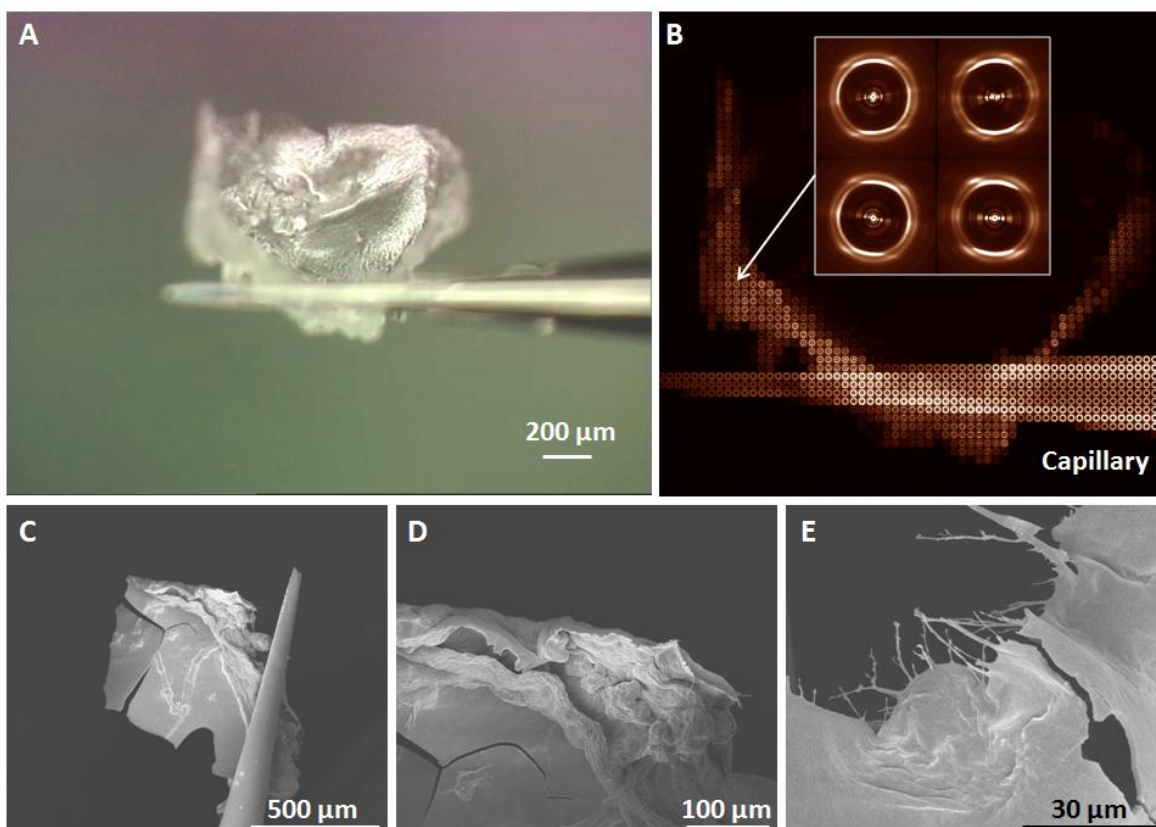
51
52 The presence of these patterns mainly concentrated in a sort of “crown” is imputable to the
53
54 pinning effect of the drying droplet as illustrated in a previous investigation of our group.^{17,28}

55
56 Indeed, after being deposited in a superhydrophobic state (*i.e.*, with a contact angle higher than
57
58
59
60

1
2
3 150°), during the evaporation process the droplet starts to shrink due to the volume reduction.
4
5 According to the aspect ratio of the surface roughness (which sustains the droplet in a
6
7 superhydrophobic state) and to the viscosity of the droplet itself (which depends on the contained
8
9 analyte, in this case A β peptide), before the end of the evaporation process the droplet dimension
10
11 becomes so small that it starts to pin the asperities, thus transiting from a superhydrophobic
12
13 “suspended” state (Cassie state) to a hydrophobic “pinned” one (Wenzel state).^{17,28} In this
14
15 configuration the droplet is not anymore in a quasi contact-free state on the substrate and this can
16
17 provoke some sensitive changes in the convective flows acting inside the droplet and in a partial
18
19 dis-homogenization of the evaporation rate. In summary, after having exploited the
20
21 homogeneous evaporation rate of the superhydrophobic state for almost the whole drying process
22
23 (the pinning effect on SHSs like the ones used here, with a CA greater than 170°, happens only
24
25 at the very end of the process), the ordered fibril material which formed during this time can get
26
27 trapped in proximity of the pinning points (Figure 6A,B) and form the “crown” illustrated by the
28
29 XRD mesh scan.
30
31
32
33
34
35

36
37 Finally, the apex of fibril boosting induced by the superhydrophobic membranes was reached
38
39 by A β (25-35). Already in its ring-like conformation, obtained with hydrophilic supports, this
40
41 fragment showed a peculiar predisposition to form amyloid fibers as illustrated in Figure 2. We
42
43 managed separating a free-standing residue from the superhydrophobic membrane and attached
44
45 it to a glass capillary for X-ray analysis (Figure 7A). A composite raster-scan image reveals that
46
47 the rim of the residue is composed of highly oriented fiber diffraction patterns (Figure 7B). A
48
49 highly structured fibrillar morphology can also be seen in scanning electron microscopy (SEM)
50
51 images (Figure 7C-E). This contrasts powder-like patterns obtained by drying solubilized A β (25-
52
53 35).⁴¹
54
55
56
57
58
59
60

1
2
3 The relatively large number of reflections exhibited by this A β fragment shows a para-
4 crystalline order similar to the one detected also for other synthetic peptides⁴² after 1 week
5 incubation time, a far longer duration if compared with our droplet evaporation protocol of about
6
7
8
9
10
11 1h.



12
13
14
15
16
17
18
19
20
21
22
23
24
25
26
27
28
29
30
31
32
33
34
35
36
37
38
39
40
41
42
43
44
45
46
47
48
49
50
51
52
53
54
55
56
57
58
59
60
Figure 7 A: Optical image of A β (25-35) free-standing residue (attached to a glass capillary tip) dried on a superhydrophobic Si₃N₄ membrane; B: μ XRD mesh scan of the residue in figure 7A (inset: close up on residue edge μ XRD patterns); C-E: SEM micrographs of the A β (25-35) residue in figure 7A.

A particularly well-ordered XRD pattern coming from the outer rim of the free-standing residue reveals an orthogonal cross- β structure with a number of equatorial peaks (Figure 8A). The a-axis is chosen along the meridional direction of the cross- β -peak and the b/c axes along the equatorial direction.⁴³ The reflection on the meridian with $d = 0.473$ nm is indexed as (100) and a $d = 0.239$ nm peak as (200) suggesting parallel β -strands (Table 1).^{19,44} The intensity profile of the cross- β peak can be separated into three h0l reflections, the (110) reflection and a

short-range order peak revealing a semicrystalline material (Figure 8B,C). The short-range order scattering ($d \sim 0.40$ nm) appears to be random. Some of the patterns in the raster-scan show only short-range order scattering due to the absence of a crystalline fraction (not shown). Subtracting such a pattern from a semicrystalline one was used to enhance the visibility of the weak equatorial peaks.

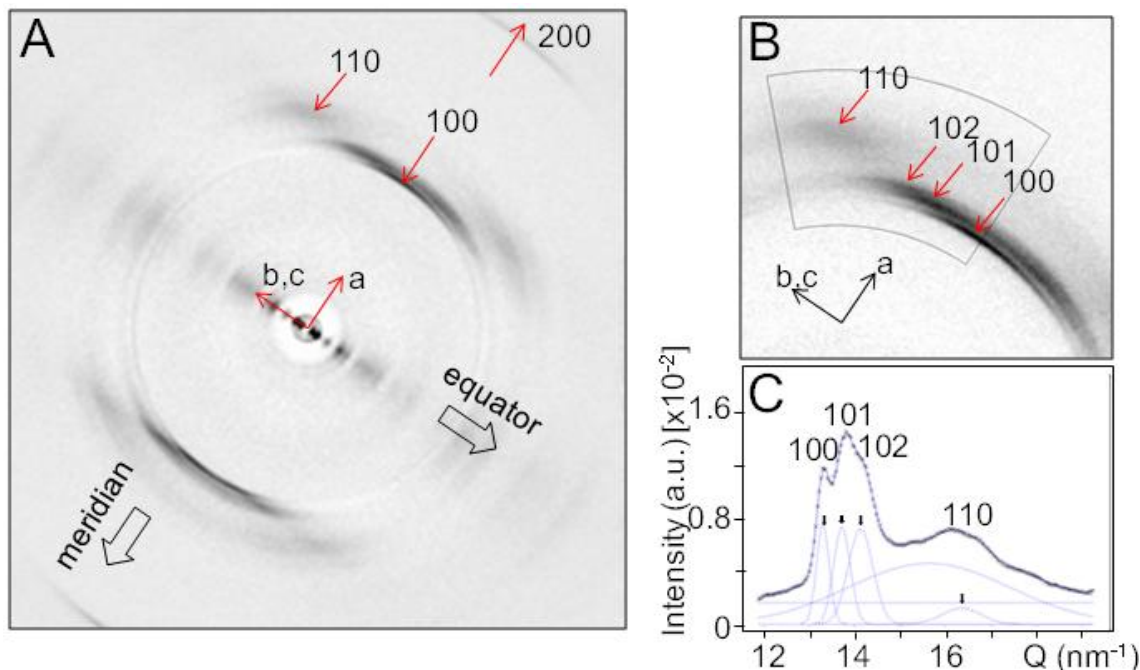


Figure 8 A: XRD pattern the A β (25-35) residue from the outer rim of the residue (Figure 7B). The reflections are indexed by an orthogonal cross- β structure. B: Zoom into cross- β -peak revealing a sub-structure due to h0l reflections and the neighboring (110) reflection. C: Radial intensity profile corresponding to the azimuthally integrated sector in (B). 4 Gaussian profiles fitted the h0l and (110) peaks (black arrows), a broad Gaussian for short-range order and a 0-order Lorentzian background. The fitted peaks and the resulting curve are in blue.

The d-spacing list and the deduced unit cell are collected in Table 1.

Table 1 A β (25-35) crystallographic parameters based on an orthogonal cross- β structure (The particle size -L- was derived from the radial peak width of fitted Gaussian functions by Scherrer's equation.⁴⁹)

hkl	d (nm)	L (nm)	Unit cell parameters ($\alpha=\beta=\gamma=90^\circ$)
(100)	0.473	25	a=0.476 nm
(200)	0.239	14	b=0.658 nm
(101)	0.458	16	c=1.833 nm
(102)	0.445	13	
(110)	0.384	7	

The b-axis of ~ 0.66 nm is shorter than expected for antiparallel β -sheets (~ 0.70 nm) supporting parallel β -sheets. The equatorial peaks extending to low-angles suggest scattering due to amyloid nanofilaments which has been studied extensively for other self-assembled oligopeptides and A β -fragments.⁴⁵⁻⁴⁷

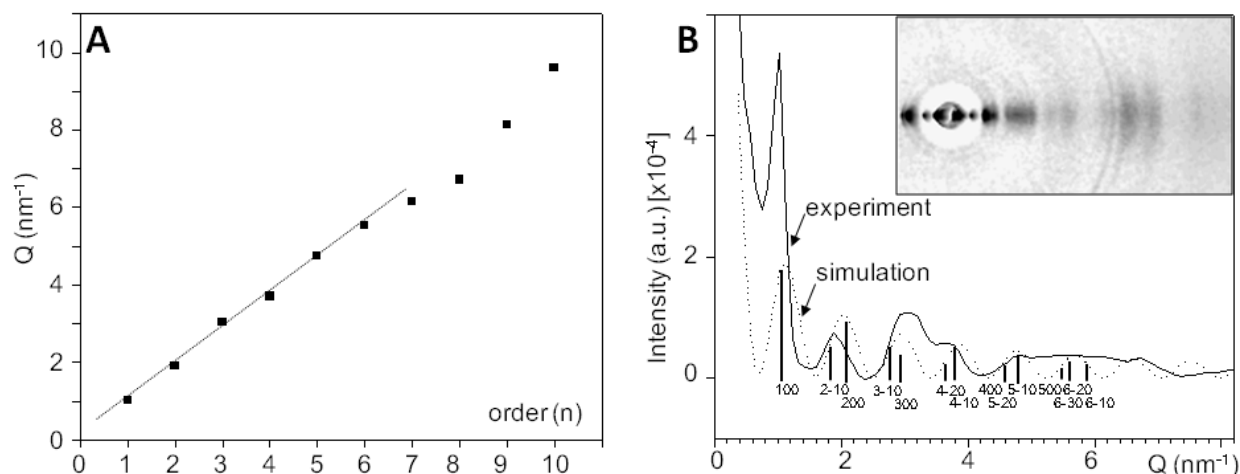


Figure 9 A: Plot of position of low-angle orders against the order number. A linear regression curve with a slope of 0.91 ($\sigma=2$) nm^{-1} has been fitted to the first 6 orders. B: Experimental intensity profile of equatorial scattering (solid line) derived by azimuthal integration across the peaks shown in the inset. Random short-range order scattering at the position of the β -peak has been subtracted in order to enhance the visibility of the peaks. The simulated scattering of a tube is shown as dotted line. The vertical bars correspond to a hexagonal lattice of close-packed tubes.⁴⁵ Only one of each set of symmetry-related reflections is shown.

The positions of the individual peaks were determined by fitting Gaussian profiles (not shown).

The orders $n=1$ to 6 show a linear Q -dependence with a slope of 0.91 ($\sigma=2$) nm^{-1} (Figure 9A). For orders $n \geq 7$ we observe a deviation from a linear dependence which is probably be due to $0kl$ equatorial reflections from the cross- β structure (Figure 9A).

The equatorial intensity trace can be modeled by a cylinder with the 6.9 ($\sigma=1$) nm diameter derived from the slope of the order plot (Figure 9; Supporting Information).^{45,47} Other models based on solid, double-walled cylinders or β -sheet slabs did not match the cylinder diameter or provided less good fits.⁴⁶ The significant difference of the calculated and observed intensities at the position of the 1st order is attributed to a coincidence of the first order interference peak of a hexagonal lattice of close-packed cylinders⁴⁸ with the form factor of the cylinder (Figure 9B).

1
2
3 The decrease of the apparent particle size (L), derived from the peak broadenings by Scherrer's
4 equation⁴⁹, of $L=38$ nm for the (100) reflection descending to 5-10 nm for the higher order
5
6 reflections supports a loss of coherence for the higher-order terms.
7
8

9
10 A less ordered equatorial trace is observed for several weaker patterns in the inner part of the
11 residue corresponding to a period of about 4.3 nm. The peaks show a larger azimuthal spread and
12 the larger peak width suggests smaller domains than for the more ordered equatorial trace. A
13 possible origin of this structural feature could be a partial melting of β -sheet strands as predicted
14 by molecular dynamics (MD) simulations.⁵⁰ The comparable weaker equatorial features suggest,
15 however, that this could only affect a small volume fraction while extensive loss of β -sheet
16 structure occurs at 309 K according to MD simulations.⁵⁰ It might therefore be interesting to
17 probe the thermal behavior of amyloid residues by combined nanocalorimetry and
18 nanodiffraction⁵¹ in the future.
19
20
21
22
23
24
25
26
27
28
29
30
31

32 **Conclusions**

33
34 In this work we showed how the presence of superhydrophobic surfaces can sensibly influence
35 the aggregation mechanisms of $A\beta$ peptides involved in the formation of fibroidal plaques at the
36 origin of Alzheimer's disease.^{3,15,16} In order to determine the structural configuration of the
37 peptides under investigation by synchrotron μ XRD techniques, we fabricated novel X-ray
38 transparent superhydrophobic Si_3N_4 membranes. Our findings show how the comparison
39 between the solid residues consisting of several $A\beta$ peptides, namely $A\beta(1-40)$, $A\beta(12-28)$ and
40 $A\beta(25-35)$, highlights peculiar conformational differences in presence of a hydrophilic or
41 superhydrophobic support. We observe a general enhancement of the fibril self-assembly
42 processes due to recirculating microfluidic flows and homogeneous evaporation rate provided by
43 superhydrorepellent surfaces.^{17,52} The quasi contact-free nature of the drying droplets allows the
44
45
46
47
48
49
50
51
52
53
54
55
56
57
58
59
60

1
2
3 formation of free-standing residues, which are homogeneously characterized by an extended
4
5 fibrillar structure if compared with the ring-like substrate-adherent moieties obtained in
6
7 hydrophilic conditions. A β (25-35) is particularly predisposed to form fiber textured structures
8
9 which resulted quasi-crystalline over the SH Si₃N₄ membrane. The protocol that we used is a
10
11 simple and straightforward method to monitor structural changes that can happen in amyloid
12
13 proteins. For this reason we envisage the extension of such study to biocompounds involved in
14
15 other neurodegenerative diseases (*e.g.* α -synuclein/Parkinson's,⁴ huntingtin/Huntington's⁵) and
16
17 non-neurodegenerative ones (*e.g.* amylin/diabetes mellitus type II^{6,7}). Further, the use of micro-
18
19 and nano-structured supports to manipulate amyloid soft matter could be also exploited as a
20
21 smart fabrication protocol for the rapid realization of amyloid fibers, which find application in
22
23 tissue engineering, cell adhesion^{29,30,34,53} and other materials applications.⁵⁴⁻⁵⁶
24
25
26
27
28
29

30 ASSOCIATED CONTENT

31
32
33 *Supporting Information Available:* Additional information on the simulation of equatorial X-ray
34
35 scattering, the experimental setup and the membranes related contact angles. This material is
36
37 available free of charge *via* the Internet at <http://pubs.acs.org>.
38
39
40

41 AUTHOR INFORMATION

42 43 44 **Corresponding Author**

45
46
47 *Dr. Angelo Accardo, Istituto Italiano di Tecnologia, angelo.accardo@iit.it, +3901071781847.
48
49

50 51 **Author Contributions**

52
53 The manuscript was written through contributions of all authors. All authors have given approval
54
55 to the final version of the manuscript.
56
57
58
59
60

ABBREVIATIONS

SHS, superhydrophobic surface; A β , Amyloid beta; TFA, trifluoro-acetic acid; μ XRD, X-ray micro-diffraction; SEM, Scanning Electron Microscopy; CA, contact angle; AD, Alzheimer's disease; PMMA, poly(methyl methacrylate); MD, molecular dynamics.

REFERENCES

- (1) Serpell, L. C.; Sunde, M.; Blake, C. C. The Molecular Basis of Amyloidosis. *Cell. Mol. Life Sci.* **1997**, *53*, 871-887.
- (2) Rambaran, R. N.; Serpell, L. C. Amyloid Fibrils: Abnormal Protein Assembly. *Prion* **2008**, *2*, 112-117.
- (3) Koo, E. H.; Lansbury, P. T. Jr.; Kelly, J. W. Amyloid Diseases: Abnormal Protein Aggregation in Neurodegeneration. *Proc. Natl. Acad. Sci. U.S.A.* **1999**, *96*, 9989-9990.
- (4) Irwin, D. J.; Lee, V. M.; Trojanowski, J. Q. Parkinson's Disease Dementia: Convergence of α -synuclein, Tau and Amyloid- β Pathologies. *Nat. Rev. Neurosci.* **2013**, *14*, 626-636.
- (5) McGowan, D. P.; van Roon-Mom, W.; Holloway, H.; Bates, G. P.; Mangiarini, L.; Cooper, G. J.; Faull, R. L.; Snell, R. G. Amyloid-like Inclusions in Huntington's Disease. *Neuroscience* **2000**, *100*, 677-680.
- (6) Westermark, P.; Andersson, A.; Westermark, G. T. Islet Amyloid Polypeptide, Islet Amyloid, and Diabetes Mellitus. *Physiol. Rev.* **2011**, *91*, 795-826.
- (7) Höppener J. W.; Lips, C. J. Role of Islet Amyloid in Type 2 Diabetes Mellitus. *Int. J. Biochem. Cell Biol.* **2006**, *38*, 726-736.
- (8) Lee, J. S.; Um, E.; Park, J. K.; Park, C. B. Microfluidic Self-assembly of Insulin Monomers into Amyloid Fibrils on a Solid Surface. *Langmuir* **2008**, *24*, 7068-7071.

- 1
2
3
4
5
6
7
8
9
10
11
12
13
14
15
16
17
18
19
20
21
22
23
24
25
26
27
28
29
30
31
32
33
34
35
36
37
38
39
40
41
42
43
44
45
46
47
48
49
50
51
52
53
54
55
56
57
58
59
60
- (9) Choi, Y. J.; Chae, S.; Kim, J. H.; Barald, K. F.; Park, J. Y.; Lee, S. H. Neurotoxic Amyloid Beta Oligomeric Assemblies Recreated in Microfluidic Platform with Interstitial Level of Slow Flow. *Sci. Rep.* **2013**, *3*, 1921.
- (10) Seidi, A.; Kaji, H.; Annabi, N.; Ostrovidov, S.; Ramalingam, M.; Khademhosseini, A. A Microfluidic-based Neurotoxin Concentration Gradient for the Generation of an *in vitro* Model of Parkinson's Disease. *Biomicrofluidics* **2011**, *5*, 22214.
- (11) Knowles, T. P. J.; White, D. A.; Abate, A. R.; Agresti, J. J.; Cohen, S. I. A.; Sperling, R. A.; De Genst, E. J.; Dobson, C. M.; Weitz, D. A. Observation of Spatial Propagation of Amyloid Assembly from Single Nuclei. *Proc. Natl. Acad. Sci. U.S.A.* **2011**, *108*, 14746–14751.
- (12) Brancolini, G.; Corazza, A.; Vuano, M.; Fogolari, F.; Mimmi, M. C.; Bellotti, V.; Stoppini, M.; Corni, S.; Esposito, G. Probing the Influence of Citrate-Capped Gold Nanoparticles on an Amyloidogenic Protein. *ACS Nano* **2015**, *9*, 2600–2613.
- (13) Chou, I. H.; Benford, M.; Beier, H. T.; Coté, G. L.; Wang, M.; Jing, N.; Kameoka, J.; Good, T. A. Nanofluidic Biosensing for Beta-amyloid Detection Using Surface Enhanced Raman Spectroscopy. *Nano Lett.* **2008**, *8*, 1729-1735.
- (14) <http://www.alz.co.uk/>
- (15) Mucke, L.; Selkoe, D. J. Neurotoxicity of Amyloid β -Protein: Synaptic and Network Dysfunction. *Cold Spring Harb. Perspect Med.* **2012**, *2*, a006338.
- (16) Walsh, D. M.; Klyubin, I.; Fadeeva, J. V.; Cullen, W. K.; Anwyl, R.; Wolfe, S.; Rowan, M. J.; Selkoe, D. J. Naturally Secreted Oligomers of Amyloid Beta Protein Potently Inhibit Hippocampal Long-term Potentiation in vivo. *Nature* **2002**, *416*, 535-539.

- 1
2
3 (17) Accardo, A.; Di Fabrizio, E.; Limongi, T.; Marinaro, G.; Riekkel, C. Probing Droplets on
4 Superhydrophobic Surfaces by Synchrotron Radiation Scattering Techniques. *J. Synchrotron*
5
6 *Radiat.* **2014**, *21*, 643–653.
7
8
9
10 (18) Accardo, A.; Shalabaeva, V.; Cotte, M.; Burghammer, M.; Krahne, R.; Riekkel, C.; Dante, S.
11 Amyloid β Peptide Conformational Changes in the Presence of a Lipid Membrane System.
12
13 *Langmuir* **2014**, *30*, 3191–3198.
14
15
16
17 (19) Accardo, A.; Shalabaeva, V.; Hesse, B.; Cotte, M.; Krahne, R.; Riekkel, C.; Dante, S.
18 Synchrotron m-FTIR highlights amyloid- β conformational changes under the effect of
19 surface wettability and external agents. *Vib. Spectrosc.* **2015**, *80*, 30-35.
20
21
22
23 (20) Pronchik, J.; He, X.; Giurleo, J. T.; Talaga D. S. In Vitro Formation of Amyloid from α -
24 Synuclein Is Dominated by Reactions at Hydrophobic Interfaces. *J. Am. Chem. Soc.* **2010**,
25 *132*, 9797-9803.
26
27
28
29
30
31 (21) Hauser, C. A.; Deng, R.; Mishra, A.; Loo, Y.; Khoe, U.; Zhuang, F.; Cheong, D. W.;
32 Accardo, A.; Sullivan, M. B.; Riekkel, C.; Ying, J. Y.; Hauser, U. A. Natural Tri- to
33 Hexapeptides Self-assemble in Water to Amyloid Beta-type Fiber Aggregates by
34 Unexpected Alpha-helical Intermediate Structures. *Proc. Natl. Acad. Sci. U.S.A.* **2011**, *108*,
35 1361-1366.
36
37
38
39
40
41
42
43 (22) Lakshmanan, A.; Cheong, D. W.; Accardo, A.; Di Fabrizio, E.; Riekkel, C.; Hauser, C. A.
44 Aliphatic Peptides Show Similar Self-assembly to Amyloid Core Sequences, Challenging
45 the Importance of Aromatic Interactions in Amyloidosis. *Proc. Natl. Acad. Sci. U.S.A.* **2013**,
46 *110*, 519-524.
47
48
49
50
51
52
53
54
55
56
57
58
59
60

- 1
2
3
4
5
6
7
8
9
10
11
12
13
14
15
16
17
18
19
20
21
22
23
24
25
26
27
28
29
30
31
32
33
34
35
36
37
38
39
40
41
42
43
44
45
46
47
48
49
50
51
52
53
54
55
56
57
58
59
60
- (23) Accardo, A.; Burghammer, M.; Di Cola, E.; Reynolds, M.; Di Fabrizio, E.; Riekkel, C. Lysozyme Fibrillation Induced by Convective Flow Under Quasi Contact-free Conditions. *Soft Matter* **2011**, *7*, 6792-6796.
- (24) Accardo, A.; Mearini, F.; Leoncini, M.; Brandi, F.; Di Cola, E.; Burghammer, M.; Riekkel, C.; Di Fabrizio, E. Fast, Active Droplet Interaction: Coalescence and Reactive Mixing Controlled by Electrowetting on a Superhydrophobic Surface. *Lab Chip* **2013**, *13*, 332-335.
- (25) Marinaro, G.; Accardo, A.; De Angelis, F.; Dane, T.; Weinhausen, B.; Burghammer, M.; Riekkel, C. A Superhydrophobic Chip Based on SU-8 Photoresist Pillars Suspended on a Silicon Nitride Membrane. *Lab Chip* **2014**, *14*, 3705-3709.
- (26) Miele, E.; Accardo, A.; Falqui, A.; Marini, M.; Giugni, A.; Leoncini, M.; De Angelis, F.; Krahne, R.; Di Fabrizio, E. Writing and Functionalisation of Suspended DNA Nanowires on Superhydrophobic Pillar Arrays. *Small* **2015**, *11*, 134-140.
- (27) Accardo, A.; Tirinato, L.; Altamura, D.; Sibillano, T.; Giannini, C.; Riekkel, C.; Di Fabrizio, E. Superhydrophobic Surfaces Allow Probing of Exosome Self Organization Using X-ray Scattering. *Nanoscale* **2013**, *5*, 2295-2299.
- (28) Accardo, A.; Gentile, F.; Mearini, F.; De Angelis, F.; Burghammer, M.; Di Fabrizio, E.; Riekkel, C. In Situ X-ray Scattering Studies of Protein Solution Droplets Drying on Micro- and Nanopatterned Superhydrophobic PMMA Surfaces. *Langmuir* **2010**, *26*, 15057-15064.
- (29) Hauser, C. A.; Zhang, S. Designer Self-assembling Peptide Nanofiber Biological Materials. *Chem. Soc. Rev.* **2010**, *39*, 2780-2790.
- (30) Hauser, C. A.; Maurer-Stroh, S.; Martins, I. C. Amyloid-based Nanosensors and Nanodevices. *Chem. Soc. Rev.* **2014**, *43*, 5326-5345.

- 1
2
3 (31) Shorter, J.; Lindquist, S. Prions as Adaptive Conduits of Memory and Inheritance. *Nat. Rev.*
4
5 *Genet.* **2005**, *6*, 435-450.
6
7
8 (32) Hu, K. N.; McGlinchey, R. P.; Wickner, R. B.; Tycko, R. Segmental Polymorphism in a
9
10 Functional Amyloid. *Biophys. J.* **2011**, *101*, 2242-2250.
11
12 (33) Rochin, L.; Hurbain, I.; Serneels, L.; Fort, C.; Watt, B.; Leblanc, P.; Marks, M. S.; De
13
14 Strooper, B.; Raposo, G.; van Niel, G. BACE2 Processes PMEL to Form the Melanosome
15
16 Amyloid Matrix in Pigment Cells. *Proc. Natl. Acad. Sci. U.S.A.* **2013**, *110*, 10658-10663.
17
18 (34) Gras, S. L.; Tickler, A. K.; Squires, A. M.; Devlin, G. L.; Horton, M. A.; Dobson, C. M.;
19
20 MacPhee, C. E. Functionalised Amyloid Fibrils for Roles in Cell Adhesion. *Biomaterials*
21
22 **2008**, *29*, 1553-1562.
23
24 (35) Deegan, R. D.; Bakajin, O.; Dupont, T. F.; Huber, G.; Nagel, S. R.; Witten, T. A. Capillary
25
26 Flow as the Cause of Ring Stains from Dried Liquid Drops. *Nature* **1997**, *389*, 827-829.
27
28 (36) Vaughan, G. B. M.; Wright, J. P.; Bytchkov, A.; Rossat, M.; Gleyzolle, H.; Snigireva, I.;
29
30 Snigirev, A. X-ray Transfocators: Focusing Devices Based on Compound Refractive Lenses.
31
32 *J. Synchrotron Radiat.* **2011**, *18*, 125-133.
33
34 (37) Kuperstein, I.; Broersen, K.; Benilova, I.; Rozenski, J.; Jonckheere, W.; Debulpaep, M.;
35
36 Vandersteen, A.; Segers-Nolten, I.; Van Der Werf, K.; Subramaniam, V.; Braeken, D.;
37
38 Callewaert, G.; Bartic, C.; D'Hooge, R.; Martins, I. C.; Rousseau, F.; Schymkowitz, J.; De
39
40 Strooper B. Neurotoxicity of Alzheimer's Disease A β Peptides is Induced by Small Changes
41
42 in the A β 42 to A β 40 Ratio. *EMBO J.* **2010**, *29*, 3408-3420.
43
44 (38) Vivekanandan, S.; Brender, J. R.; Lee, S. Y.; Ramamoorthy, A. A Partially Folded
45
46 Structure of Amyloid-Beta(1-40) in an Aqueous Environment. *Biochem. Biophys. Res.*
47
48 *Commun.* **2011**, *411*, 312-316.
49
50
51
52
53
54
55
56
57
58
59
60

- 1
2
3
4
5
6
7
8
9
10
11
12
13
14
15
16
17
18
19
20
21
22
23
24
25
26
27
28
29
30
31
32
33
34
35
36
37
38
39
40
41
42
43
44
45
46
47
48
49
50
51
52
53
54
55
56
57
58
59
60
- (39) Canale, C.; Seghezza, S.; Vilasi, S.; Carrotta, R.; Bulone, D.; Diaspro, A.; San Biagio, P. L.; Dante, S. Different Effects of Alzheimer's Peptide A β (1–40) Oligomers and Fibrils on Supported Lipid Membranes. *Biophys. Chem.* **2013**, *182*, 23–29.
- (40) Millucci, L.; Raggiaschi, R.; Franceschini, D.; Terstappen, G.; Santucci, A. Rapid Aggregation and Assembly in Aqueous Solution of A β (25-35) Peptide. *J. Biosci.* **2009**, *34*, 293-303.
- (41) Bond, J. P.; Deverin, S. P.; Inouye, H.; El-Agnaf, O. M. A.; Teeter, M. M.; Kirschner, D. A. Assemblies of Alzheimer's Peptides A β 25–35 and A β 31–35: Reverse-Turn Conformation and Side Chain Interactions Revealed by X-Ray Diffraction. *J. Struct. Biol.* **2003**, *141*, 156-170.
- (42) Morris, K. L.; Rodger, A.; Hicks, M. R.; Debulpaep, M.; Schymkowitz, J.; Rousseau, F.; Serpell, L. C. Exploring the Sequence–structure Relationship for Amyloid Peptides. *Biochem. J.* **2013**, *450*, 275-283.
- (43) Weisman, S.; Okada, S.; Mudie, S. T.; Huson, M. C.; Trueman, H. E.; Sriskantha, A.; Haritos, V. S.; Sutherland, T. D. Fifty Years Later: The Sequence, Structure and Function of Lacewing Cross-Beta Silk. *J. Struct. Biol.* **2009**, *168*, 467-475.
- (44) Serpell, L. C. Alzheimer's amyloid fibrils: structure and assembly. *Biochim. Biophys. Acta* **2000**, *1502*, 16-30.
- (45) Inouye, H.; Fraser, P. E.; Kirschner, D. A. Structure of β -Crystallite Assembly Formed by Alzheimer β -Amyloid Protein Analogues: Analysis by X-Ray Diffraction. *Biophys. J.* **1993**, *64*, 502-519.
- (46) Inouye, H.; Sharma, D.; Goux, W. J.; Kirschner, D. A. Structure of Core Domain of Fibril-Forming PHF/Tau Fragments. *Biophys. J.* **2006**, *90*, 1774–1789.

- 1
2
3 (47) Malinchik, S. B.; Inouye, H.; Szumowski, K. E.; Kirschner, D. A. Structural Analysis of
4 Alzheimer's $\beta(1-40)$ Amyloid: Protofilament Assembly of Tubular Fibrils. *Biophys. J.* **1998**,
5
6 74, 537-545.
7
8
9
10 (48) Oster, G.; Riley, D. P. Scattering from Cylindrically Symmetric Systems. *Acta Cryst.* **1952**,
11
12 5, 272-276.
13
14
15 (49) Klug, H. P.; Alexander, L. E. *X-ray Diffraction Procedures for Polycrystalline and*
16
17 *Amorphous Materials*. 2nd ed.; Wiley Interscience: New York, N.Y., 1974.
18
19
20 (50) Duka, V.; Czaplewski, C.; Segalen, V; Liepina, I. Molecular Modeling of Single Beta-Sheet
21
22 and the Beta-Sheet Stack of Amyloid Protein 25-35. *Materials Sciences and Applied*
23
24 *Chemistry* **2011**, 23, 62-72.
25
26
27 (51) Riekel, C.; Di Cola, E.; Reynolds, M.; Burghammer, M.; Rosenthal, M.; Doblaz, D.; Ivanov,
28
29 D. A. Thermal Transformations of Self-assembled Gold Glyconanoparticles Probed by
30
31 Combined Nanocalorimetry and X-ray Nanobeam Scattering. *Langmuir* **2015**, 31, 529-534.
32
33
34 (52) Marinaro, G.; Accardo, A.; Benseny-Cases, N.; Burghammer, M.; Castillo-Michel, H.;
35
36 Cotte, M.; Dante, S.; Angelis, F. D.; Cola, E. D.; Di Fabrizio, E.; Hauser, C.; Riekel, C.
37
38 Probing Droplets with Biological Colloidal Suspensions on Smart Surfaces by Synchrotron
39
40 Radiation Micro- and Nano-Beams. *Opt. Lasers Eng.* **2015**, DOI:
41
42 10.1016/j.optlaseng.2015.03.004.
43
44
45 (53) Alsteens, D.; Ramsook, C. B.; Lipke, P. N.; Dufrière, Y. F. Unzipping a Functional
46
47 Microbial Amyloid. *ACS Nano* **2012**, 6, 7703–7711.
48
49
50 (54) Peralta, M. D.; Karsai, A.; Ngo, A.; Sierra, C.; Fong, K. T.; Hayre, N. R.; Mirzaee, N.;
51
52 Ravikumar K. M.; Kluber, A. J.; Chen, X.; Gang-yu, L. Y.; Toney, M. D.; Singh, R. R.;
53
54
55
56
57
58
59
60

Cox, D. L. Engineering Amyloid Fibrils from β -solenoid Proteins for Biomaterials Applications. *ACS Nano* **2015**, *9*, 449-463.

(55) Varongchayakul, N.; Johnson, S.; Quabili, T.; Cappello, J.; Ghandehari, H.; De Jesus Solares, S.; Hwang, W.; Seog, J. Direct Observation of Amyloid Nucleation under Nanomechanical Stretching. *ACS Nano* **2013**, *7*, 7734–7743.

(56) Yang, H.; Fung, S.Y.; Pritzker, M.; Chen, P. Surface-assisted Assembly of an Ionic-complementary Peptide: Controllable Growth of Nanofibers. *J. Am. Chem. Soc.* **2007**, *129*, 12200-12210.

Graphical Table of Contents

